Accepted for publication in The Astrophysical Journal
Preprint typeset using LaTeX style emulateapj v. 5/2/11

arXiv:1409.7693v1 [astro-ph.GA] 26 Sep 2014

CLUSTERING OF MODERATE LUMINOSITY X-RAY SELECTED TYPE 1 AND TYPE 2 AGN AT Z∼3

V. Allevato[1], A. Finoguenov[1,2], F. Civano[3,4] N. Cappelluti[5,2], F. Shankar[6,7] T. Miyaji[8,9], G. Hasinger[10], R. Gilli[5], G. Zamorani[5], G. Lanzuisi[11], M. Salvato[12], M. Elvis[4], A. Comastri [5] & J. Silverman[13]

Accepted for publication in The Astrophysical Journal

ABSTRACT

We investigate, for the first time at z∼3, the clustering properties of 189 Type 1 and 157 Type 2 X-ray active galactic nuclei (AGN) of moderate luminosity ($\langle L_{bol}\rangle = 10^{45.3}$ erg s^{-1}), with photometric or spectroscopic redshifts in the range 2.2<z<6.8. These samples are based on *Chandra* and *XMM-Newton* data in COSMOS. We find that Type 1 and Type 2 COSMOS AGN at z∼3 inhabit DMHs with typical mass of $\log M_h = 12.84^{+0.10}_{-0.11}$ and $11.73^{+0.39}_{-0.45}$ h^{-1}M$_\odot$, respectively. This result requires a drop in the halo masses of Type 1 and 2 COSMOS AGN at z∼3 compared to $z\lesssim 2$ XMM COSMOS AGN with similar luminosities. Additionally, we infer that unobscured COSMOS AGN at z∼3 reside in 10 times more massive halos compared to obscured COSMOS AGN, at 2.6σ level. This result extends to z∼3 that found in COSMOS at $z\lesssim 2$, and rules out the picture in which obscuration is purely an orientation effect. A model which assumes that the AGN activity is triggered by major mergers is quite successful in predicting both the low halo mass of COSMOS AGN and the typical mass of luminous SDSS quasars at z ∼ 3, with the latter inhabiting more massive halos respect to moderate luminosity AGN. Alternatively we can argue, at least for Type 1 COSMOS AGN, that they are possibly representative of an early phase of fast (i.e. Eddington limited) BH growth induced by cosmic cold flows or disk instabilities. Given the moderate luminosity, these new fast growing BHs have masses of $\sim 10^{7-8}$ M$_\odot$ at z∼3 which might evolve into $\sim 10^{8.5-9}$ M$_\odot$ mass BHs at z=0. Following our clustering measurements, we argue that this fast BH growth at z∼3 in AGN with moderate luminosity occurs in DMHs with typical mass of $\sim 6\times10^{12}$ h^{-1}M$_\odot$.

Subject headings: Surveys - Galaxies: active - X-rays: general - Cosmology: Large-scale structure of Universe - Dark Matter

1. INTRODUCTION

The connection between black holes (BHs) and their host dark matter halos (DMHs) has been mainly studied via clustering measurements of active galactic nuclei (AGN). Under an assumed cosmology, the AGN bias (i.e. the square root of the relative amplitude of AGN clustering to that of dark matter, e.g., Kaiser 1984) can be inferred and linked to the typical mass of AGN hosting DMHs (e.g., Jing 1998; Sheth & Tormen 1999, Sheth et al. 2001, Tinker et al. 2005, 2010). This provides information about galaxy/AGN co-evolution and the mechanisms that trigger the AGN activity.

The clustering properties of thousands of broad-line luminous quasars with typical $L_{bol} \gtrsim 10^{46}$ erg s^{-1}, have been studied in different large area optical surveys, such as 2QZ (e.g. Croom et al. 2005; da Angela et al. 2005; Porciani & Norberg 2006), SDSS (e.g., Shen et al. 2009; Ross et al. 2009) and 2SLAQ (Croom et al. 2009; da Angela et al. 2008). All these studies suggest the common picture that luminous optically selected quasars are hosted by halos of roughly constant mass, a few times 10^{12} M$_\odot$ h^{-1}, out to z∼3-4. This lack of variation in halo mass implies that the bias factor is an increasing function of redshift, since the DM is more weakly clustered earlier in cosmic time.

In addition, quasar clustering measurements have also facilitated several theoretical investigations on the cosmic evolution of BHs within the hierarchical structure formation paradigm (e.g., Hopkins et al. 2007; Shankar et al. 2008a, 2008b; White et al. 2008; Croton 2008; Wyithe & Loeb 2008). Interestingly, models of major mergers between gas-rich galaxies appear to naturally produce the evolution of the quasar large-scale bias as a function of luminosity and redshift (Hopkins et al. 2007, 2008; Shen 2009; Shankar et al. 2009, 2010; Bonoli et al. 2009). This supports the scenario in which major mergers dominate the luminous quasar population (Scannapieco et al. 2004, Shankar 2010, Neistein & Netzer 2013,

[1] Department of Physics, University of Helsinki, Gustaf Hällströmin katu 2a, FI-00014 Helsinki, Finland
[2] University of Maryland, Baltimore County, 1000 Hilltop Circle, Baltimore, MD 21250, USA
[3] Department of Physics and Astronomy, Dartmouth College, 6127 Wilder Laboratory, Hanover, NH 03755
[4] Harvard Smithsonian Center for Astrophysics, 60 Garden Street, Cambridge, MA 02138, USA
[5] INAF-Osservatorio Astronomico di Bologna, Via Ranzani 1, 40127 Bologna, Italy
[6] Department of Physics and Astronomy, University of Southampton, Highfield, SO17 1BJ
[7] GEPI, Observatoire de Paris, CNRS, Univ. Paris Diderot, 5 Place Jules Janssen, F-92195 Meudon, France
[8] Instituto de Astronomia, Universidad Nacional Autonoma de Mexico, Ensenada, Mexico (mailing adress: PO Box 439027, San Ysidro, CA, 92143-9024, USA)
[9] Center for Astrophysics and Space Sciences, University of California at San Diego, Code 0424, 9500 Gilman Drive, La Jolla, CA 92093, USA
[10] Institute for Astronomy, University of Hawaii, 2680 Woodlawn Drive, Honolulu, HI 96822, USA
[11] National Observatory of Athens I.Metaxa & Vas. Pavlou St. GR-15236 Penteli, GREECE
[12] Max-Planck-Institute für Extraterrestrische Physik, Giessenbachstrasse 1, D-85748 Garching, Germany
[13] Institute for the Physics and Mathematics of the Universe, The University of Tokyo, 5-1-5 Kashiwanoha, Kashiwashi, Chiba 277-8583, Japan

Treister et al. 2012).

X-ray detection is generally recognized as a more robust way to obtain a uniformly selected AGN sample with lower luminosities ($L_{bol} \sim 10^{44-46}$ erg s^{-1}) and with a significant fraction of obscured sources with respect to optical surveys. This means that while deep X-ray AGN samples are from square-degree area surveys, sampling moderate luminosity AGN, optical quasars are from thousands of square degree surveys, sampling rare and high luminosity AGN events. Thanks to *Chandra* and *XMM-Newton* surveys, large samples of X-ray AGN are available and clustering measurements of moderate luminosity AGN are now possible with a precision comparable to that achievable with quasar redshift surveys.

Measurements of the spatial clustering of X-ray AGN show that they are located in galaxy group-sized DMHs with $\log M_h$ = 13-13.5 h^{-1}M$_\odot$ at low (∼0.1) and high (∼ 1-2) redshift (e.g. Hickox et al. 2009, Cappelluti et al. 2010, Allevato et al. 2011, Krumpe et al. 2010, 2012, Mountrichas et al. 2012, Koutoulidis et al. 2013).

The fact that DMH masses of this class of moderate luminosity AGN are estimated to be, on average, 5-10 times larger than those of luminous quasars, has been interpreted as evidence against cold gas accretion via major mergers in those systems (e.g. Allevato et al. 2011; Mountrichas & Georgakakis 2012). Additionally, it has been explained as support for multiple modes of BH accretion (cold versus hot accretion mode, e.g. Fanidakis et al. 2013). However, this difference, which may not be present at z<0.7 (Krumpe et al. 2012) does not yet have a good explanation.

On the other hand, several works on the morphology of the AGN host galaxies suggest that, even at moderate luminosities, a large fraction of AGN is not associated with morphologically disturbed galaxies. This trend has been observed both at low (z∼1, e.g. Georgakakis et al. 2009, Cisternas et al. 2011) and high (z∼2, e.g. Schawinski et al. 2011, Rosario et al. 2011, Kocevski et al. 2012) redshift.

Despite the power of clustering measurements in understanding AGN population, little is known about the clustering of obscured AGN. These sources, based on the results from deep X-ray surveys (e.g. Brandt & Hasinger 2005; Tozzi et al. 2006) and X-ray background synthesis models (e.g. Civano et al. 2005, Gilli et al. 2007), are the most abundant AGN population in the Universe. Additionally, they are expected to dominate the history of accretion onto SMBHs (e.g. Fabian & Iwasawa 1999). A basic prediction of orientation-driven AGN unification models is that the clustering strength should be similar for obscured (narrow-line or Type 2) and unobscured (broad-line or Type 1) AGN. By contrast, in the AGN evolutionary scenario, obscured quasars may represent an early evolutionary phase after a major merger event, when the growing BHs can not produce a high enough accretion luminosity to expel the surrounding material (e.g., Hopkins et al. 2008; King 2010). Following this argument, the luminous quasar phase might probably correspond to the end of an obscured phase. On the other hand, if the AGN activity is triggered by sporadic gas inflow, not by major mergers, then obscured and unobscured AGN might be two stages that may occur several times along the galaxy lifetime. The different durations of these two stages and their relation to the environment may produce different clustering properties between obscured and unobscured AGN (Hickox et al. 2011).

Some studies of optically selected quasars confirm that low-redshift narrow-line AGN are not strongly clustered and are hosted in galaxies that do not differ significantly from typical non-AGN galaxies (e.g., Wake et al. 2004, Magliocchetti et al. 2004, Mandelbaum et al. 2009; Li et al. 2006). Hickox et al. (2011), analysing a sample of 806 Spitzer mid-IR-selected quasars at $0.7 < z < 1.8$ in the Bootes field, find marginal ($< 2\sigma$) evidence that obscured quasars have a larger bias and populate more massive DMHs than unobscured quasars. Recently, Donoso et al. (2013) using mid-IR-WISE selected AGN candidates at z∼1.1, infer that red AGN (i.e obscured sources) are hosted by massive DMHs of $\log M_h \sim 13.5$ h^{-1}M$_\odot$. This value is well above the halo mass of $\log M_h \sim 12.4$ h^{-1}M$_\odot$ that harbour blue AGN (unobscured sources).

On the contrary, Krumpe et al. (2012) find no significant difference in the clustering of X-ray narrow-line and broad-line RASS AGN at 0.07<z<0.5. A larger clustering amplitude for Type 1 with respect to Type 2 AGN, has been observed in the Swift- BAT all sky survey at z∼0 (Cappelluti et al. 2010). The redshift evolution of the bias of moderate luminosity X-ray AGN have been investigated in Allevato et al. (2011) by using XMM COSMOS data. They find that the bias increases with redshift tracing a constant halo mass typical of galaxy groups ($\sim 10^{13}$ h^{-1}M$_\odot$) up to z∼2. Additionally, their results indicate that obscured XMM COSMOS AGN inhabit slightly (2.3σ) less massive halos than unobscured sources.

The clustering of AGN at $z > 2$ is still poorly investigated. At high redshifts galaxies and AGN are thought to form in rare peaks of the density field and then to be strongly biased relative to the DM (Kaiser 1984; Bardeen et al. 1986). The clustering of $z > 2.9$ SDSS quasars (Shen et al. 2007, 2009) indicates (with large uncertainties on the bias) that luminous quasars reside in massive halos with mass few times 10^{13} h^{-1}M$_\odot$. Following Shankar et al. (2010), these clustering measurements require a high duty cycle (i.e. the probability for an AGN of being active at a given time) for massive BHs ($> 10^9 M_\odot$) in luminous quasars ($L_{bol} > 10^{46}$ erg s^{-1}). The clustering signal measured by Shen et al. (2009) at z=3.2 has also been interpreted with the halo occupation distribution (HOD) by Richardson et al. (2012). Given the large uncertainty of the signal at z=3.2, especially at small scales, they only infer the mass of central halos hosting quasars ($M_{cen}=14.1^{+5.8}_{-6.9} \times 10^{12}$ h^{-1}M$_\odot$).

The clustering of moderate luminosity X-ray AGN at $z \geqslant 2$ is indeed largely unexplored. The only attempt of measuring the clustering properties of X-ray AGN at z=3 is presented in Francke et al. (2008). They estimate the correlation function of a small sample of X-ray AGN with $L_{bol} \sim 10^{44.8}$ erg s^{-1}, in the Extended Chandra Deep Field South (ECDFS). They find indications that X-ray ECDFS AGN reside in DMHs with minimum mass of $\log M_{min} = 12.6^{+0.5}_{-0.8}$ h^{-1} M$_\odot$. Unfortunately, because of the small number of sources, the bias factor has a very large uncertainty.

In this paper we use a larger sample of X-ray selected AGN with $L_{bol} \sim 10^{45.3}$ erg s^{-1}, based on *Chandra* and *XMM-Newton* data in the COSMOS field, at 2.2<z<6.8.

The purpose is to measure the clustering amplitude and the typical hosting halo mass of moderate luminosity AGN at z $\sim$ 3. Additionally, we focus on the measurements of the large-scale bias of Type 1 and Type 2 COSMOS AGN at z $\geqslant$ 2.2. This redshift range has never been explored before for the clustering of moderate luminosity obscured and unobscured sources. Throughout the paper, all distances are measured in comoving coordinates and are given in units of Mpc h^{-1}, where $h = H_0/100$km/s. We use a ΛCDM cosmology with $\Omega_M = 0.3$, $\Omega_\Lambda = 0.7$, $\Omega_b = 0.045$, $\sigma_8 = 0.8$. The symbol *log* signifies a base-10 logarithm.

2. AGN CATALOG

The *Cosmic Evolution Survey* (COSMOS, Scoville et al. 2007) is a panchromatic photometric and spectroscopic survey of 2 deg^2 of the equatorial sky, observed by the most advanced astronomical facilities, with imaging data from X-ray to radio. The inner part of the COSMOS field ($\sim$ 0.92 deg^2) has been imaged for a total of 1.8 Ms by *Chandra*, while XMM-*Newton* surveyed 2.13 deg^2, for a total of $\sim$ 1.55 Ms. Large samples of point-like X-ray sources detected in the 0.5-10 keV energy band, are presented in the *Chandra*-COSMOS (C-COSMOS) point-like source catalog (1761 objects; Elvis et al 2009, Civano et al. 2012) and in the XMM COSMOS multiwavelength catalog (1822 objects; Cappelluti et al. 2009, Brusa et al. 2010). Of the 1822 XMM COSMOS sources, 945 have been detected by *Chandra*. Extensive spectroscopic campaigns have been carried out in the field, providing a total of 890 and 1069 unique, good quality spectroscopic redshifts (spec-zs) for XMM COSMOS and C-COSMOS sources, respectively. In addition, photometric redshifts (phot-zs) for all the XMM COSMOS sources and for $\sim$96% of the C-COSMOS sources have been obtained exploiting the COSMOS multiwavelength database and are presented in Salvato et al. (2009, 2011).

The prime interest of this paper is to investigate the clustering properties of X-ray AGN at z$\sim$3. To this end, we use the catalog of C-COSMOS sources and we limit to a sample of 252 AGN detected in the soft band, with phot or spec-zs, when available, $\geq$ 2.2. In addition, we include in the analysis 94 AGN with spec or phot-zs $\gtrsim$2.2, which are outside the inner region observed by *Chandra* and then XMM-only detected. Then the final sample includes a total of 346 COSMOS AGN.

The spectroscopic or photometric classification is available for each AGN on the basis of a combined X-ray and optical classification if spectra are available, or by the type of template that best fits the photometry of the source. We classify as Type 1 those sources with at least one broad (FWHM $>$ 2000 km s^{-1}) emission line in their spectra or fitted with the template of an unobscured AGN. On the contrary, Type 2 AGN are defined as sources showing narrow emission lines or absorption lines only, or well fitted by an obscured AGN template. More details on this classification method are presented in Brusa et al. (2010) and Civano et al. (2012). Following the criteria described above, 189/346 and 157/346 COSMOS AGN have been classified as Type 1 and Type 2 , respectively.

The intrinsic 2-10 keV rest-frame luminosity, corrected for absorption, is known for all the XMM COSMOS sources from the X-ray spectral analysis as described in Mainieri et al. (2007) and Lanzuisi et al. (2013). Unfortunately, for C-COSMOS AGN the X-ray spectral analysis can be performed for only a few bright sources. However, at z$>$2, the hardness ratio is a good measure of the presence of high column densities and absorption. For this reason, we use the hardness ratios known for all the C-COSMOS sources to derive the absorption column density and then the de-absorbed X-ray luminosities. In detail, for each C-COSMOS AGN, we derive the rest frame luminosity from the soft flux, assuming a power-law model with Γ=1.8. The Galactic absorption is set to $N_{H,Gal}$=2.6$\times$10^{20} cm^{-2}, i.e. the value in the direction of the COSMOS field (Kalberla et al. 2005). The rest frame luminosity is then corrected for the intrinsic absorption using the hardness ratio.

Finally, we derive the bolometric luminosities for the entire sample of 346 COSMOS AGN using the bolometric correction k_{bol} quoted in Lusso et al. (2012, see Table 2). In this conversion, we properly take into account the different classification of the sources (Type 1 or Type 2) and the band of the de-absorbed rest-frame X-ray luminosity.

As shown in Figure 1, the intrinsic bolometric luminosity of the entire sample of 346 COSMOS AGN, spans $\sim$ 3 order of magnitude, from 10^{44} to $\sim$10^{47} erg s^{-1}. The mean and the dispersion of the distribution are (45.3, 0.6) in log and in unit of erg s^{-1}. Therefore, this sample is dominated by moderate luminosity X-ray AGN with a mean bolometric luminosity $\sim$ 2 orders of magnitude lower than that of luminous optical quasars at similar redshift (Shen et al. 2009). Due to the lower limiting flux of *Chandra* with respect to XMM detections, the distribution of bolometric luminosities of C-COSMOS AGN peaks at lower values. The intrinsic L_{bol} distributions of 189 Type 1 and 157 Type 2 COSMOS AGN are shown in Figure 2, with mean and dispersion equal to (45.47, 0.58) and (45.15, 0.58) for Type 1 and 2, respectively (in log and units of erg s^{-1}).

In order to evaluate the effect of using photometric redshifts in the clustering measurements, we also construct a sample of 138 COSMOS AGN detected in the soft band, with available spec-zs $\geq$ 2.2. The redshift and intrinsic bolometric luminosity distributions for this sample are shown in Figure 1 and the corresponding mean values are quoted in Table 1. Following the spectroscopic classification, the sample has been divided onto 107 Type 1 and 31 Type 2 COSMOS AGN (see Figure 2).

3. 2PCF AND AGN BIAS FACTOR

Measurement of the two-point correlation function (2PCF) requires the construction of a random catalog with the same selection criteria and observational effects as the real data. To this end, we construct a random catalog where each simulated source is placed at a random position in the sky, with flux randomly extracted from the catalog of real source fluxes (e.g. Gilli et al. 2009, Allevato et al. 2011). Following this method, the simulated source is kept in the random sample if its flux is above the sensitivity map value at that position (Miyaji et al. 2007; Cappelluti et al. 2009). We prefer this method with respect to the one that keeps the angular coordinates unchanged as that approach has the disadvantage of removing the contribution to the signal due to angu-

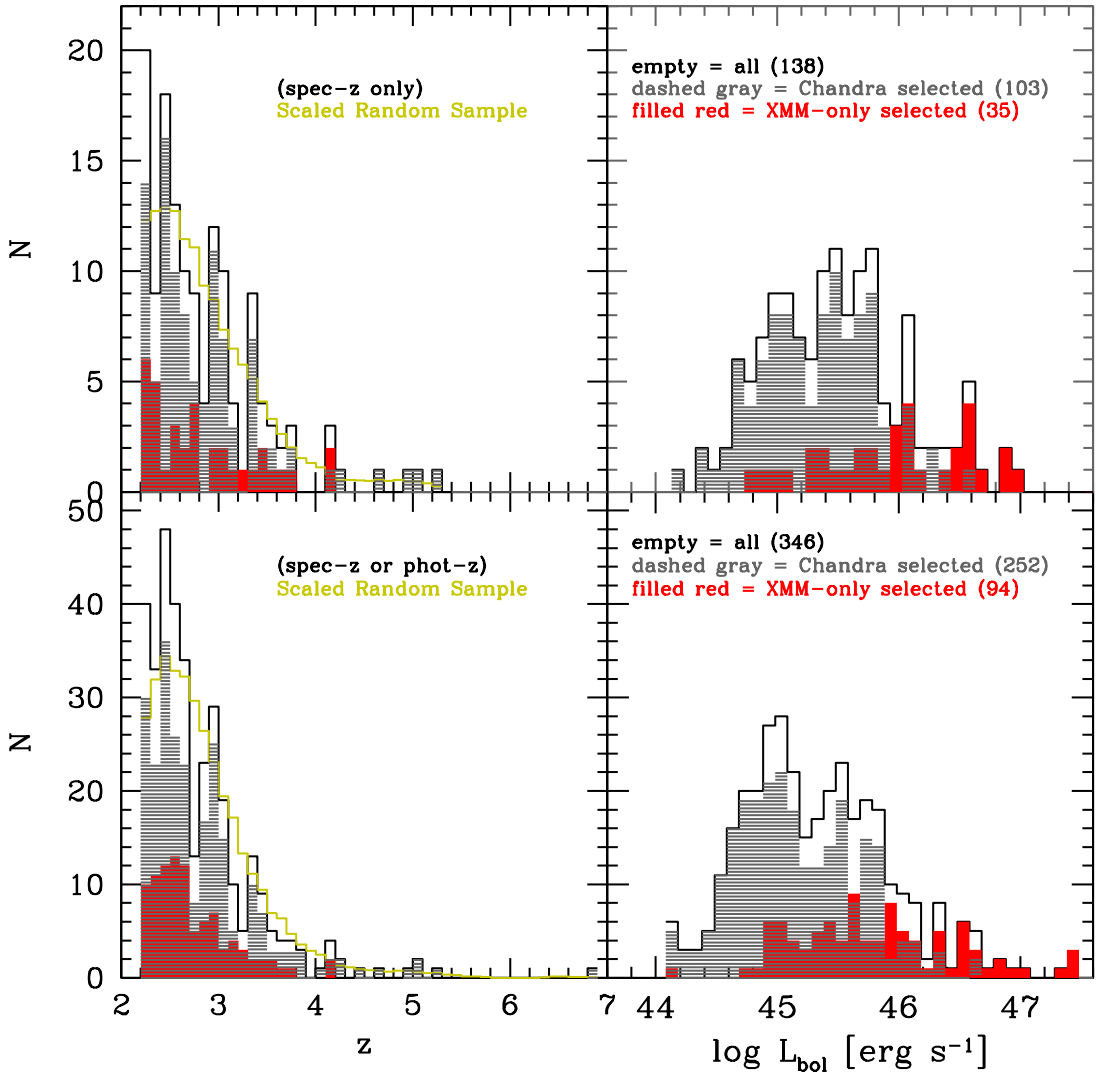

FIG. 1.— Redshift and intrinsic bolometric luminosity distributions of *Chandra*-COSMOS AGN (dashed gray histogram), XMM-only selected AGN (filled red histogram) and of the combined catalog (solid black histogram) of 138 COSMOS AGN with known spec-zs $\geqslant$2.2 (upper quadrants) and of 346 COSMOS AGN with known spec or phot-zs $\geqslant$2.2 (lower quadrants). The empty gold histograms in the left panels show the redshift distributions of the random catalogs obtained using a Gaussian smoothing with σ=0.2.

lar clustering. Nevertheless, Gilli et al. (2005, 2009) and Koutoulidis et al. (2013) have shown that there is only a small difference ($\sim$15%) in the clustering signal derived with the two different procedures.

The corresponding redshifts of the random objects are assigned based on the smoothed redshift distribution of the real AGN sample. Specifically, we assume a Gaussian smoothing length $\sigma_z = 0.2$. This is a good compromise between scales that are too small, which would suffer from local density variations, and those that are too large, which would oversmooth the distribution. The redshift distribution of COSMOS AGN and of the random samples are shown in Figure 1.

We estimate the projected 2PCF function $w_p(r_p)$ by using (Davis & Peebles 1983):

$$w_{AGN}(r_p) = 2\int_0^{\pi_{max}} \xi(r_p,\pi)d\pi \qquad (1)$$

where $\xi(r_p,\pi)$ is defined in Landy & Szalay (1993, LS) as:

$$\xi = \frac{1}{RR}[DD - 2DR + RR] \qquad (2)$$

The LS estimator is described as the ratio between AGN pairs in the data sample and those in the random catalog, as a function of the projected comoving separations between the objects (in the directions perpendicular, r_p and parallel, π to the line-of-sight). The choice of π_{max} is a compromise between having an optimal signal-to-noise ratio and reducing the excess noise from high separations. Usually, the optimum π_{max} value can be determined by estimating $w_p(r_p)$ for different values of π_{max} and finding the value at which the 2PCF levels off. Following this approach, we fixed $\pi_{max} = 100$ h^{-1}Mpc in estimating the 2PCF of 346 COSMOS AGN with known spec or phot-zs. For the smaller sample of 138 COSMOS AGN

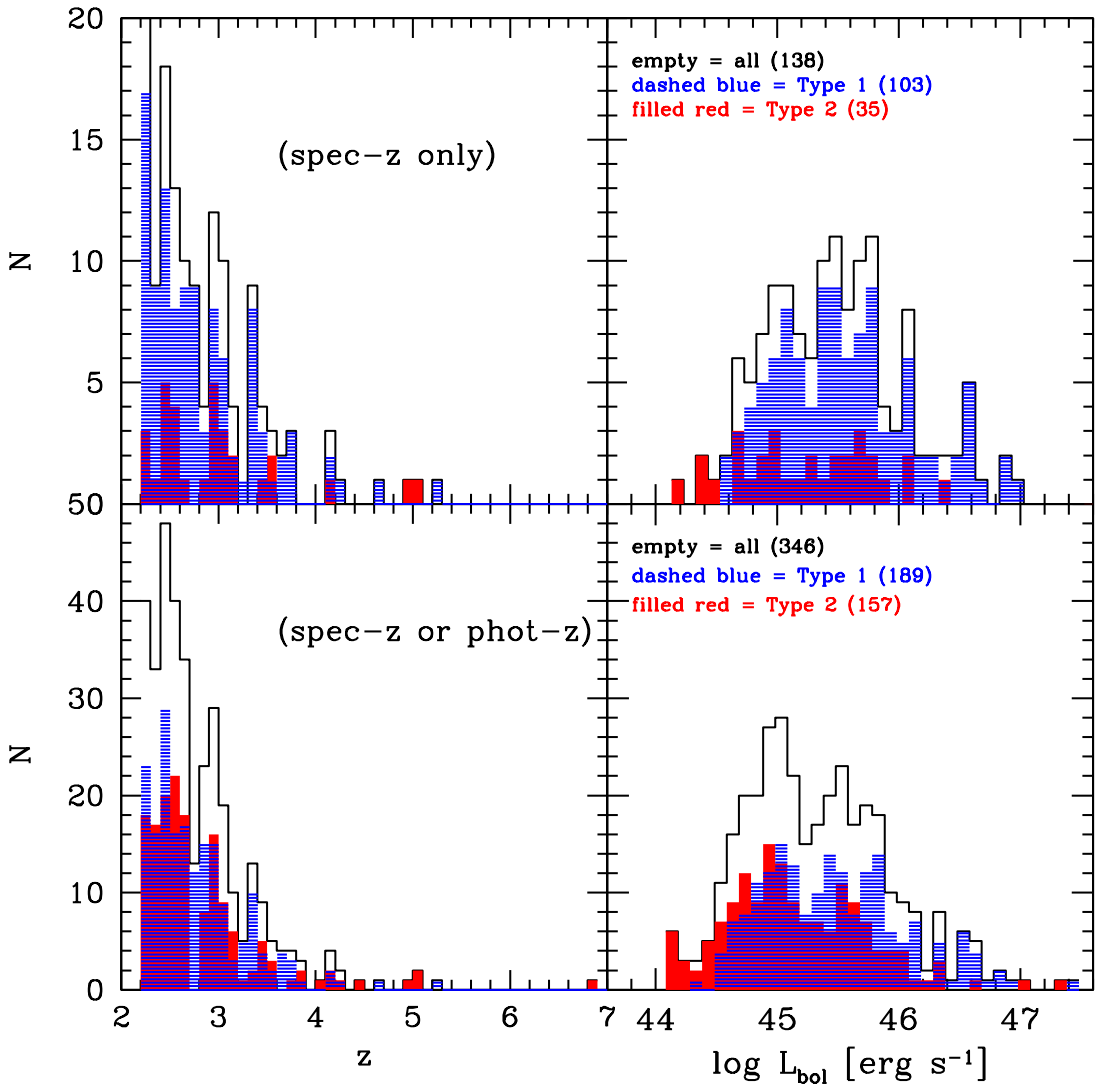

FIG. 2.— Redshift and intrinsic bolometric luminosity distributions of Type 1 AGN (dashed blue histogram), Type 2 AGN (filled red histogram) and of the combined catalog (solid black histogram) of 138 COSMOS AGN with known spec-zs ⩾2.2 (upper quadrants) and of 346 COSMOS AGN with known spec or phot-zs ⩾2.2 (lower quadrants). The mean values of the distributions are quoted in Table 1.

with available spec-zs, we set $\pi_{max} = 40$ h^{-1}Mpc. The larger π_{max} adopted in the former case is due to the use of phot-zs.

In the halo model approach (e.g. Miyaji et al. 2011, Krumpe et al. 2012), the 2PCF is modelled as the sum of contributions from AGN pairs within individual DMHs (1-halo term, $r_p < 1$ Mpc h^{-1}) and in different DMHs (2-halo term, $r_p \gtrsim 1$ Mpc h^{-1}). The superposition of the two terms describes the shape of the observed 2PCF. In this context, the bias parameter b reflects the amplitude of the AGN 2-halo term relative to the underlying DM distribution, i.e.:

$$w_{mod}(r_p, z) = b^2 w_{DM}^{2-h}(r_p, z) \quad (3)$$

We first estimate the DM 2-halo term at the mean redshift of the sample, using:

$$w_{DM}^{2-h}(r_p) = r_p \int_{r_p}^{\infty} \frac{\xi_{DM}^{2-h}(r) r dr}{\sqrt{r^2 - r_p^2}} \quad (4)$$

where

$$\xi_{DM}^{2-h}(r) = \frac{1}{2\pi^2} \int P^{2-h}(k) k^2 \left[\frac{sin(kr)}{kr}\right] dk \quad (5)$$

$P^{2-h}(k)$ is the Fourier Transform of the linear power spectrum, assuming a power spectrum shape parameter $\Gamma = 0.2$ which corresponds to $h = 0.7$.

4. RESULTS

4.1. *Bias Factors and DMH masses*

The projected 2PCF function $w_p(r_p)$ of 346 COSMOS AGN is shown in the left panel of Figure 3, in the range

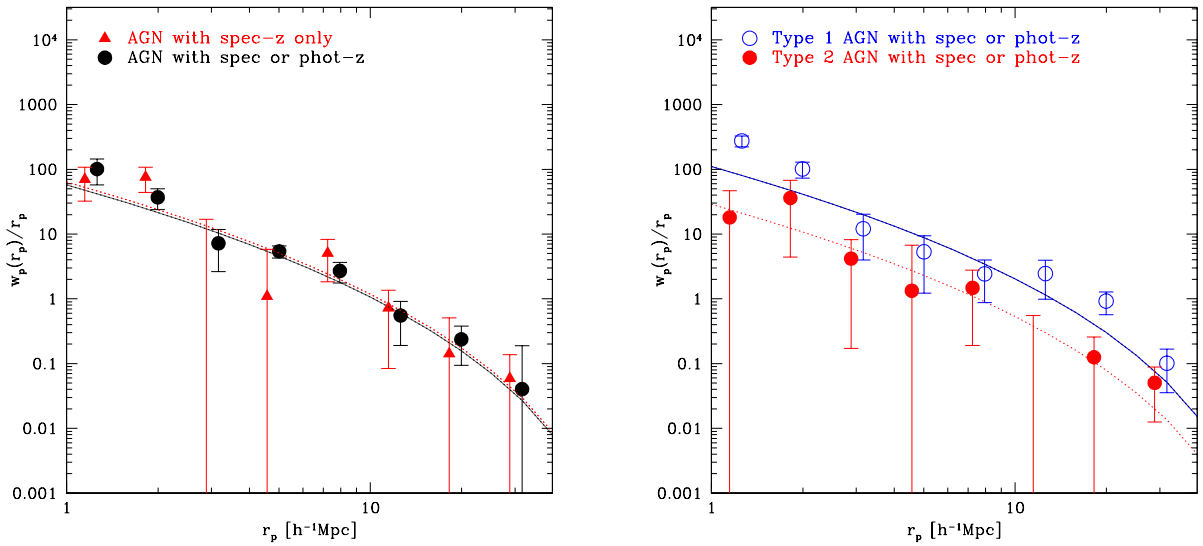

FIG. 3.— Left Panel: Projected 2PCF of 346 COSMOS AGN with phot or spec-zs, when available, $\gtrsim$ 2.2 (black circles) and 138 COSMOS AGN with known spec-zs $\gtrsim$ 2.2 (red triangles). The 1σ errors on $w_p(r_p)$ are the square root of the diagonal components of the covariance matrix, which quantifies the level of correlation between different bins. Right panel: Projected 2PCF of 189 Type 1 (blue empty circles) and 157 Type 2 (red circles) COSMOS AGN with known spec or phot-zs $\gtrsim$ 2.2. The lines mark the AGN 2-halo term as defined in Equation 3, i.e. $b^2 w_{DM}^{2-h}(r_p)$, where $w_{DM}(r_p)$ is the DM 2-halo term evaluated at the mean redshift of the samples.

TABLE 1
PROPERTIES OF THE AGN SAMPLES

Sample	N z>2.2	$\langle z \rangle$	log $\langle L_{BOL} \rangle$ erg s^{-1}	b	logM$_h$ h^{-1}M$_\odot$
			Only spec-zs		
All AGN	138	2.86	45.50	$3.94^{+0.45}_{-0.46}$	$12.36^{+0.17}_{-0.21}$
Type 1	107	2.82	45.58	$4.93^{+0.55}_{-0.52}$	$12.75^{+0.15}_{-0.16}$
Type 2	31	2.96	45.22	...	...
			Spec or phot-z		
All AGN	346	2.8	45.32	$3.85^{+0.21}_{-0.22}$	$12.37^{+0.10}_{-0.09}$
Type 1	189	2.79	45.47	$5.26^{+0.35}_{-0.39}$	$12.84^{+0.10}_{-0.11}$
Type 2	157	2.81	45.15	$2.69^{+0.62}_{-0.69}$	$11.73^{+0.39}_{-0.45}$

of r_p = 1-30 h^{-1} Mpc. The 1σ errors on $w_p(r_p)$ are the square root of the diagonal components of the covariance matrix (Miyaji et al. 2007, Krumpe et al. 2010), which quantifies the level of correlation between different bins. Following Eq. 3, we derive the best-fit bias by using a χ^2 minimization technique with 1 free parameter, where $\chi^2 = \Delta^T M_{cov}^{-1} \Delta$. In detail, Δ is a vector composed of $w_{AGN}(r_p) - w_{mod}(r_p)$ (see Equations 1 and 3), Δ^T is its transpose and M_{cov}^{-1} is the inverse of covariance matrix. The latter is used in the fit to take into account the correlation between errors. We find that, at $\langle z \rangle$=2.8, COSMOS AGN have a bias of b=$3.85^{+0.21}_{-0.22}$, where the 1σ errors correspond to $\Delta\chi^2 = 1$.

We then relate the large-scale bias to a typical mass of the hosting halos, following the bias-mass relation $b(M_h, z)$ defined by the ellipsoidal collapse model of Shen et al. (2001) and the analytical approximation of van den Bosch (2002). We find that COSMOS AGN at $\langle z \rangle$=2.8 inhabit DMHs with log M$_h$ = $12.37^{+0.10}_{-0.09}$.

Usually, phot-zs are characterized by large uncertainty. Hickox et al. (2012) showed that, even uncertainties of σ_z=0.25(1+z) cause the clustering amplitude of AGN cross-correlated with galaxies in the Bootes field, to decrease by only ∼10 per cent. COSMOS AGN has the advantage that, at z>2, $\sigma_z/(1+z) < 0.05$ (Salvato et al. 2011). Hence we do not expect a significant difference from the 2PCF derived using only spec-zs.

In order to verify this, we measure the clustering signal for a smaller sample of 138 COSMOS AGN with available spec-zs ≥2.2. The left panel of Figure 3 compares the projected 2PCFs estimated with the two different AGN samples. As expected, by using a larger AGN sample with both phot-zs and spec-zs, we improve the statistics and so the quality of the signal. However, we find consistent bias factors, irrespective of including photometric redshifts (see Table 1). This result suggests that the use of a significant fraction of AGN with known phot-zs is not affecting the result systematically. Instead, we are improving the statistics, almost tripling the number of AGN.

We investigate whether Type 1 COSMOS AGN are more strongly clustered than Type 2 objects, as already observed at low redshift (e.g. Cappelluti et al. 2010, Allevato et al. 2011). The right panel of Fig. 3 shows the projected 2PCF of Type 1 and Type 2 AGN with known phot and spec-zs ≥2.2. We find that unobscured COSMOS AGN reside in more massive halos compared to obscured AGN. In fact, we measure a best-fit bias equal to b$_{unob}$=$5.26^{+0.35}_{-0.39}$ for Type 1 and b$_{ob}$=$2.69^{+0.62}_{-0.69}$ for Type 2 AGN, respectively. These bias factors correspond to typical DMH masses of logM$_h$= $12.84^{+0.10}_{-0.11}$ and logM$_h$= $11.73^{+0.39}_{-0.45}$ h^{-1}M$_\odot$, respectively.

We check that the bias factor of Type 1 COSMOS AGN does not change when limiting the analysis to a sample of 107 unobscured sources with available spec-zs ≥2.2. Unfortunately, we cannot test the effect of phot-zs in measuring the 2PCF of obscured sources, given the small number of Type 2 objects (31) with spec-zs ≥2.2. The

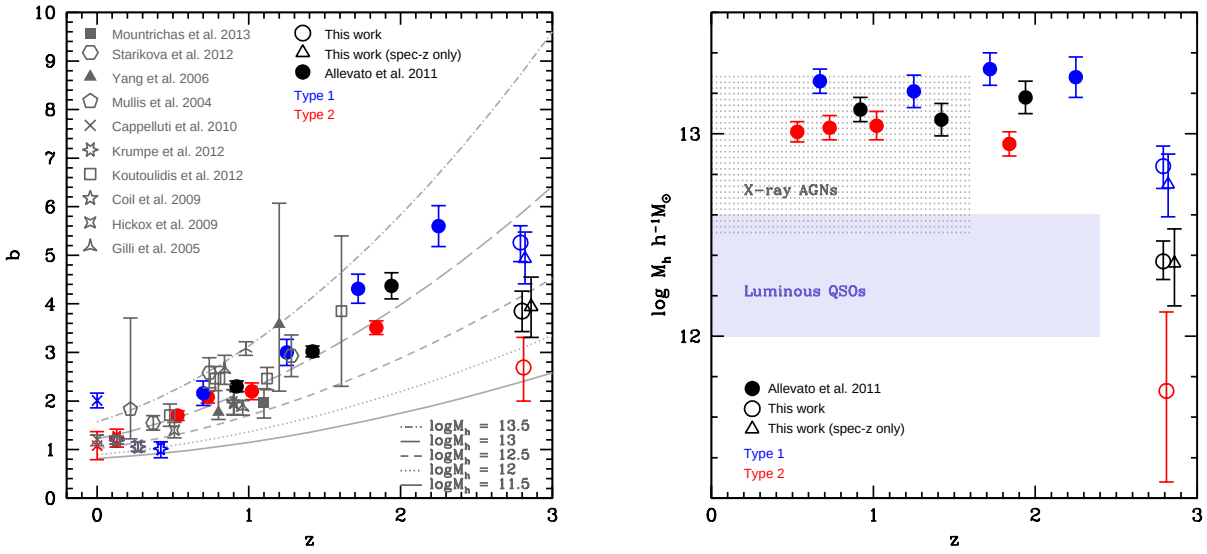

FIG. 4.— Left Panel: Bias factor as a function of redshift for moderate luminosity X-ray selected (grey), Type 1 (blue) and Type 2 (red) AGN, as derived in previous works according to the legend. The empty triangles and circles at z∼3 mark the bias factors of our sample of moderate luminosity COSMOS AGN as estimated in this work. For comparison, the filled circles show the bias derived in Allevato et al. (2011) at z$\lesssim$2.2 for XMM COSMOS AGN with similar luminosities. The dotted lines underline the expected redshift evolution of the bias of DMHs with constant mass of 11.5, 12, 12.5, 13, 13.5 h^{-1} $M_\odot$ in log scale and in unit of $M_\odot h^{-1}$ (from bottom to top). The bias-mass relation is based on the ellipsoidal collapse model of Sheth et al. (2001). Right Panel: Corresponding typical DMH mass of our sample of COSMOS AGN at z∼3, divided in Type 1 (blue) and Type 2 (red) AGN, estimated following the bias-mass relation b(Mh,z) described in van den Bosch (2002) and Sheth et al. (2001). For comparison, the filled circles mark the redshift evolution of the typical DMH mass of XMM COSMOS AGN at z$\lesssim$2.2, as derived in Allevato et al. (2011). The halo mass range is shown also for optically selected luminous quasars (shaded region, Croom et al. 2005, Porciani et al. 2004, Myers et al. 2006, Shen et al. 2009, Ross et al. 2009, da Angela et al. 2008), and X-ray selected AGN (dotted shaded region, Gilli et al. 2005, Coil et al. 2009, Cappelluti et al. 2010, Allevato et al. 2011, Krumpe et al. 2010, 2012, Hickox et al. 2009, Mountricas et al. 2013, Koutoulidis et al. 2012, Starikova et al. 2012).

best-fit bias factors and the corresponding typical DMH masses for each subsample of COSMOS AGN used in this work are shown in Table 1.

4.2. *Redshift Evolution of the AGN bias*

The left panel of Figure 4 shows the bias factors derived for our sample of COSMOS AGN at z∼3, along with a collection of values estimated in previous studies at lower redshifts. The different lines mark the redshift evolution of the bias corresponding to different constant DMH masses, as predicted by the ellipsoidal collapse model of Sheth et al. (2001). The filled circles show the redshift evolution of the bias for a comparable sample of moderate luminosity XMM COSMOS AGN at z$\lesssim$2, as presented in Allevato et al. (2011).

The right panel of Figure 4 shows the redshift evolution of the corresponding typical DMH masses derived following the bias-mass relation defined by the ellipsoidal collapse model of Shen et al. (2001). The general picture at z$\lesssim$2 is that the bias of moderate luminosity X-ray AGN increases with redshift tracing a constant group-sized halo mass. Allevato et al. (2011) have shown that XMM COSMOS AGN (with $L_{bol} \sim 10^{45.2}$ erg s^{-1}) reside in DMHs with constant mass equal to $\log M_h = 13.12\pm0.07$ h^{-1} $M_\odot$ up to z∼2 (Figure 4, filled black points).

By contrast, at z∼3, we found that our COSMOS AGN with similar luminosities, inhabit less massive DMHs (Figure 4, open black points) with $\log M_h = 12.37^{+0.10}_{-0.09}$ $h^{-1}M_\odot$. This result is significant at the 6.2σ level.

A similar trend has been observed for both Type 1 and Type 2 COSMOS AGN. Allevato et al. (2011) found that unobscured AGN reside in slightly more massive halos than obscured AGN up to z∼2.2 ($\log M_h = 13.28\pm0.07$ and 13.00 ± 0.06 $h^{-1}M_\odot$, respectively). Instead, our results at z∼3 require, compared to z$\lesssim$2 results, a drop in the halo mass to $\log M_h = 12.84^{+0.10}_{-0.11}$ (3.6σ result) and $11.73^{+0.39}_{-0.45}$ $h^{-1}M_\odot$ (3σ result) for Type 1 and Type 2 COSMOS AGN.

5. DISCUSSION

In the following sections we will discuss our results and we will attempt to answer the question why the redshift evolution of the bias changes at z$\geqslant$ 2.2.

First of all we note that the number density of 10^{13} $h^{-1}M_\odot$ mass halos tends to evolve faster beyond z∼3, with a progressive drop in the abundance of massive (and rarer) host halos at high redshifts. This fact alone suggests a possible increase with redshift in the ratio between the BH mass and host halo mass, with a mapping of moderate luminosity AGN in progressively less massive halos at higher redshift. Independent studies support such a type of evolution (e.g. White, Martini & Cohn 2008, Shankar et al. 2010).

5.1. *Major merger models at z ∼ 3*

In this section we try to explain our clustering measurements at z∼3 within hierarchical mergers scenario.

Figure 5 shows a collection of bias estimates for broad-line optically selected SDSS quasars at z=3.2 (Shen et al. 2009), X-ray selected AGN in the ECDFS at z=3 (Francke et al. 2008) and the results presented in this work, as a function of L_{bol}. For our data points, the errors

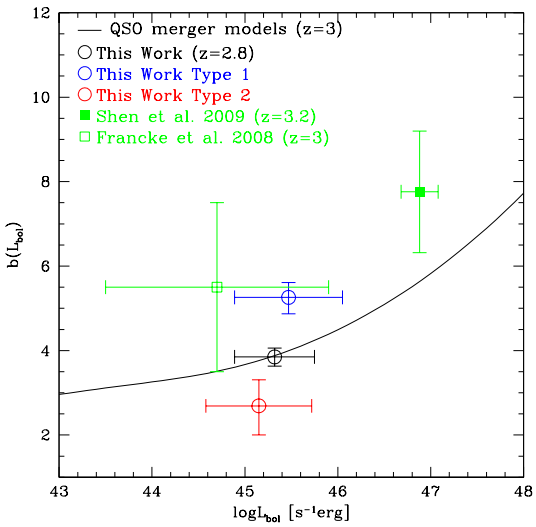

FIG. 5.— Bias factor as a function of bolometric luminosity for optically selected SDSS quasars at z=3.2 (Shen et al. 2009, green squares), X-ray selected AGN in the ECDFS at z=3 (Francke et al. 2008, green open square) and our results according to the legend. For our data points, the errors on the L_{bol} axis correspond to the dispersion of the bolometric luminosity distributions of each subset. The continuous line shows the luminosity evolution of the bias at z = 3, predicted with the theoretical model of Shen (2009), which assumes a quasar phase triggered by a major merger (see the text for more details).

on the L_{bol} axis correspond to the dispersion of the bolometric luminosity distributions for the different subsets. Our sample of COSMOS AGN and X-ray ECDFS AGN with slightly lower luminosities, have consistent bias factors within 1σ. However, our estimate has significantly smaller uncertainty, given the larger number of sources used in the analysis. On the contrary, Shen et al. (2009) measured a slightly higher bias ($<2\sigma$) for luminous Type 1 quasars with bolometric luminosity $\sim$ 2 orders of magnitude higher with respect to our sample of unobscured AGN.

The continuous line marks the predicted bias as a function of bolometric luminosity, computed according to the framework of the growth and evolution of SMBHs presented in Shen (2009, see also Shankar 2010) at z = 3. Their model assumes that quasar activity is triggered by major mergers of host halos (e.g. Kauffmann & Haehnelt 2000). In addition, they assume that the resulting AGN light curve follows a universal form with its peak luminosity correlated with the (post-)merger halo mass.

The major merger model was adapted to fully reproduce the optical/X-ray data at z<2-3 (Shankar et al. 2010, Allevato et al. 2011). With no additional fine-tuning the major merger model is quite successful in predicting the bias of COSMOS AGN at z$\sim$3 as a function of bolometric luminosity and it is in broad agreement with the data points. The drop in the typical DMH mass to few times 10^{12} $M_{\odot}h^{-1}$ can then be explained assuming that, unlike z$\lesssim$2 XMM COSMOS AGN, COSMOS AGN at z$\sim$3 are triggered by galaxy major mergers.

In addition, the major merger model predicts a luminosity-dependent bias, with more luminous AGN inhabiting more massive DMHs. The evolution of the bias with the bolometric luminosity traced by the data marginally confirms this trend. It is important to note that at lower redshifts the bolometric luminosity dependence is significantly milder (e.g. Myers et al. 2006, Shen et al. 2009) or even reversed (e.g. Allevato et al. 2011), with moderate luminosity AGN residing in more massive DMHs with respect to luminous quasars. Such an evolutionary trend is difficult to reconcile with AGN triggering models, at different redshifts, based only on major mergers (Bournaud et al. 2011, Fanidakis et al. 2013, Di Matteo et al. 2011).

In the framework of the BH growth presented in Fanidakis et al. (2013, 2013a), our results at z$\sim$ 3 can be interpreted in terms of absence of interplay between cold and hot-halo mode. In fact, they suggest the picture that, in the z$\sim$3-4 Universe, the cold accretion mode (accretion during disk instabilities and galaxy mergers) is solely responsible for determining the environment of moderate luminosity AGN, while the AGN feedback is switched off. Our results confirm that z$\sim$3 is the epoch when the hot-halo mode is still a negligible fuelling channel. At lower redshifts both accretion modes have to be taken into account. The hot halo mode becomes prominent only in DM haloes with masses greater than $\sim 10^{12.5}$ $h^{-1}M_{\odot}$, where AGN feedback typically operates.

5.2. *Fast growing BHs at z ∼ 3*

A major merger model can broadly reproduce the clustering of moderate luminosity AGN at z$\sim$3. This is because mergers are most efficient in halos of masses around $\sim 3\times10^{12}$ $M_{\odot}$, which is the typical mass scale inferred from our direct clustering measurements. However, this is not a proof of uniqueness of merger models as an explanation of our results. Major galaxy mergers are not a requirement for efficient fuel supply and growth, particularly for the earliest BHs. Alternatively, an early phase of fast BH growth could be induced by cosmic cold flows (e.g. Dekel et al. 2009, Di Matteo et al. 2012, Dubois et al. 2012) or disk instabilities (e.g. Bournaud et al. 2012). Cold flows and disk instabilities in high redshift disk galaxies operate on short time scales (unlike secular processes in low-z disks). In addition, they are efficient, producing a mass inflow similar to a major merger but spread over a longer period (then the duty cycle is higher).

Different BH accretion models (e.g. Marconi et al. 2004, Merloni et al. 2008, Shankar et al. 2004,2009,2013, Bournaud et al. 2011, Fanidakis et al. 2013, Di Matteo et al. 2011) broadly agree that $z \gtrsim 2$ is the epoch of rapid growth for both low and high-mass BHs. This conclusion holds irrespective of uncertainties in duty cycle, AGN luminosity functions, or even input Eddington ratio distributions. Figure 6 shows the average accretion history of different BH masses as described in Marconi et al. (2004) and Shankar et al. (2013).

Due to the flux and volume limits of our survey, our sample of Type 1 COSMOS AGN at z$\sim$3 mainly includes moderate luminosity sources with $L_{bol} \sim 10^{45}$ erg s^{-1}. Thus, it excludes low-luminosity AGN with typical BH mass $\lesssim 10^{6-7}M_{\odot}$, or even bright quasars associated to very massive BHs ($> 10^{8-9}M_{\odot}$) and $L_{bol} > 10^{46}$ erg s^{-1}. This means that our sample of Type 1 COSMOS AGN is possibly representative of AGN corresponding to raising population of fast (i.e. Eddington limited) growing BHs with masses of $\sim 10^{7-8}$ $M_{\odot}$ at z$\sim$3.

According to the BH accretion histories shown in Fig 6, these fast growing $\sim 10^{7-8}$ $M_\odot$ mass BHs evolve in BHs with mass of the order of $\sim 10^{8.5-9}$ $M_\odot$ at z=0. This picture is consistent with the fact that moderate luminosity Type 1 AGN in zCOSMOS at z=1-2.2 (black circle in Figure 6) have BH masses in the range $M_{BH}=10^{8-9}$ $M_\odot$ with Eddington ratios λ=0.01-1, as shown in Merloni et al. (2010).

Following our results, we can argue that these fast growing BHs at z∼3 reside in DMHs with typical mass of $\sim 10^{12.8}$ $h^{-1}M_\odot$, which is the mass inferred for Type 1 COSMOS AGN hosting halos. Between z∼3 and z∼2 the typical halo mass of Type 1 COSMOS AGN increases. The BH accretion models suggest that these AGN are also rapidly growing their BH mass. The duty cycle and Eddington ratio, which are close to unity at z∼3, then decline with decreasing redshift. This leads to a strong evolution of the number density of X-ray AGN at $z\gtrsim 3$ as observed in COSMOS (Brusa et al. 2010, Civano et al. 2011), albeit for an AGN sample including both Type 1 and 2 objects.

The picture is completely different at z<2, where the bias of Type 1 AGN starts to follow the constant DMH mass track. The growth of BHs becomes more sub-Eddington (e.g., Vittorini et al. 2005, Shankar et al. 2013, and references therein) and their mass saturates to a constant value down to $z = 0$ (Figure 6). This flat host halo mass at $z\lesssim 2$ for X-ray AGN with moderate luminosity might be due to high mass halos switching to radio-loud, X-ray weak ($< 10^{44}$ erg s^{-1}) AGN. This limits the X-ray AGN population with moderate luminosity to halos with masses $\lesssim 10^{13}$ $M_\odot$. A plausible mechanism is that AGN feedback prevents gas from cooling in very massive halos. These radiatively inefficient, jet-dominated outbursts may be fueled by accretion directly from the hot gas halo and so are only possible in massive galaxies with large hosting halos (e.g. Fanidakis et al. 2011, 2012, 2013).

The picture described above for Type 1 COSMOS AGN representative, of new fast-growing BHs at z∼3, may or may not be valid for Type 2 COSMOS AGN. In fact, for the latter, we do not know the typical mass of the central BHs at any redshift. However, it is not unreasonable to assume that for Type 2 AGN, the observed redshift evolution of the bias reflects lower massive BHs and DMH masses with respect to Type 1 AGN. Lower massive halos are more abundant at z∼3 and are characterized by a slower redshift evolution of the number density. The increase of the fraction of obscured AGN with redshift (e.g. Hasinger 2008, Merloni et al. 2014) supports this scenario in which Type 1 and Type 2 objects follow different DMH mass tracks as a function of redshift.

5.3. *Type 1 vs Type 2 AGN*

In this section we discuss the clustering properties of 189 Type 1 and 157 Type 2 COSMOS AGN with phot or spec-zs, when available, $\gtrsim 2.2$.

We find a strong indication that unobscured AGN reside in 10 times more massive halos (see Table 1) with respect to obscured sources (3σ result). A difference in clustering between obscured and unobscured quasars rules out the simplest unified models (e.g. Urry & Padovani 1995) in which obscuration is purely an orientation effect.

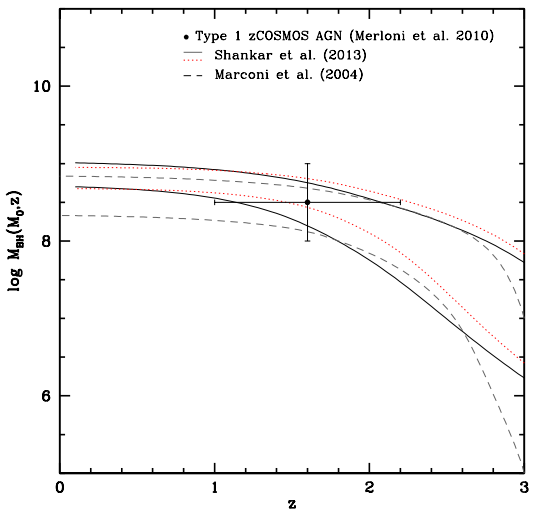

FIG. 6.— Average accretion history of BHs of different mass M_0 at z = 0 as a function of redshift. The black continuous (red dotted) line marks a model with a redshift-independent (dependent) Gaussian distribution of the Eddington ratio with a fixed radiative efficiency (Shankar et al. 2013). The black dashed line shows the growth history of BHs described in Marconi et al. (2004) with given starting mass at z = 3 computed using the Ueda et al. (2003) luminosity function and fixed duty cycle and radiative efficiency. The data point shows Type 1 zCOSMOS AGN in the redshift range 1<z< 2.2 presented in Merloni et al. (2010) with BH masses in the range $M_{BH}=10^{8-9}$ $M_\odot$ and Eddington ratios λ=0.01-1.

Type 1 and Type 2 COSMOS AGN have slightly different luminosities. However, the difference in the bias factors between Type 1 and Type 2 AGN can not be explained in terms of luminosity-dependent bias predicted by major merger models. The curve in Figure 5 predicts a milder change of bias with luminosity in the range $\log L_{bol} = 45.1 - 45.5$ erg s^{-1}.

This result would extend to z∼3 that found for z<2 Type 1 and Type 2 XMM COSMOS AGN with similar luminosities (Allevato et al. 2011).

6. CONCLUSIONS

We use a sample of 346 moderate luminosity ($\langle L_{bol}\rangle = 10^{45.3}$ erg s^{-1}) COSMOS AGN based on *Chandra* and *XMM-Newton* data, with known spec or phot-zs in the range 2.2<z<6.8. Our main goal is to measure clustering amplitudes and to estimate characteristic DM halo masses at $z \sim 3$. We also obtain, for the first time at $z \sim 3$, a highly significant clustering signal for Type 1 and Type 2 COSMOS AGN. This redshift range has never been used before to investigate the clustering of obscured and unobscured AGN, at these luminosities. We model the 2PCF of COSMOS AGN with the halo model, which relates the large-scale bias to the amplitude of the AGN 2-halo term relative to the underlying DM distribution. We translate the bias factor into a typical mass of the hosting halos, following the bias-mass relation defined by the ellipsoidal collapse model of Sheth et al. (2001). Key results can be summarized as follows.

1. At z∼3 Type 1 and Type 2 COSMOS AGN inhabit DMHs with typical mass of $\log M_h = 12.84^{+0.10}_{-0.11}$ and $11.73^{+0.39}_{-0.45}$ $h^{-1}M_\odot$. This result requires a drop in

the halo masses at z∼3 compared to z$\lesssim$2 XMM COSMOS AGN with similar luminosities.

2. At z∼3 Type 1 COSMOS AGN reside in ∼10 times more massive halos compared to Type 2 COSMOS AGN, at 2.6σ level. This result extends to z∼3 that found in COSMOS at z$\lesssim$2, and rules out the picture in which obscuration is purely an orientation effect.

3. A plausible explanation of the drop in the halo mass of COSMOS AGN might be that these moderate luminosity sources at z $\sim$ 3 are triggered by galaxy major mergers. In fact, major merger models are quite successful in predicting the halo mass of COSMOS AGN and luminous SDSS quasars at z $\sim$ 3, with the latter inhabiting more massive halos with respect to moderate luminosity AGN.

4. Alternatively, we can argue that, at least for Type 1 COSMOS AGN, they are possibly representative of moderate luminosity AGN associated to an early phase of fast (i.e. Eddington limited) BH growth induced by, for instance, cosmic cold flows or disk instabilities. According with BH accretion models, these new fast growing BHs have masses of $\sim 10^{7-8}$ $M_\odot$ at z∼3 which might evolve into $\sim 10^{8.5-9}$ $M_\odot$ mass BHs at z=0.

5. Following our clustering measurements, we argue that this fast BH growth at z∼3, in Type 1 AGN with moderate luminosity, occurs in DMHs with typical mass of $\sim 6\times10^{12}$ $h^{-1}M_\odot$.

Improving our understanding of the AGN triggering mechanisms at z $\sim$ 3 and beyond using AGN clustering measurements requires larger dataset. The COSMOS Legacy survey (Civano et al. 2014, submitted) with 1.45 deg^2 at 2×10^{-16} erg/cm^2/s will provide the largest survey at this depth ever performed. This will let us constrain the faint end of the AGN luminosity function and of the BH mass functions at z>3. This regime, which is not otherwise sampled, will allow us to understand the BH growth in the early universe and to study the clustering properties of $\sim$ 350 expected luminous quasars and L^* AGN at 3<z<6.

We thank the referee for a very helpful report. We gratefully acknowledge the contributions of the entire COSMOS collaboration consisting of more than 100 scientists. More information on the COSMOS survey is available at http://www.astro.caltech.edu/COSMOS. VA and AF wish to acknowledge Finnish Academy award, decision 266918. FC aknowledges the support of NASA contract 11-ADAP11- 0218. FS acknowledges partial support from a Marie Curie grant. TM acknowledges supports from UNAM-PAPIIT 104113 and CONACyT Grant 179662. We thank Alessandro Marconi for providing the tracks shown in Figure 5 and John Regan for helpful discussions.

REFERENCES

Allevato V., et al. 2011, ApJ, 736, 99
Brusa, M., Civano, F., Comastri, A., et al., 2010, ApJ, 716, 348
Cappelluti, N., Brusa M., Hasinger G., et al., 2009, A&A, 497, 635
Cappelluti, N., Aiello M., Burlon D., et al., 2010, ApJ, 716, 209
Coil, A. L., Georgakakis, A., Newman, J. A., et al. 2009, ApJ 701 1484
da Ângela, J., Shanks, T., Croom, S. M., et al. 2008, MNRAS, 383, 565
Davis, M., Peebles, P. J. E., 1983, ApJ, 267, 465
Donoso, E., Yan, Lin, Stern, D., Assef, R. J., 2013, 2013arXiv1309.2277D
Elvis, M., Chandra-COSMOS Team, 2007, in Bullettin of the American Astronomical Society, Vol. 39, p.899
Elvis M., Civano F., Vignani C., et al. 2009, ApJS, 184, 158
Fanidakis, N., et al. 2013, MNRAS, 435, 679
Francke, H., et al. 2008, ApJ, 673, 13
Fry, J. N., 1996, ApJ, 461, 65
Georgakakis, A., Coil, A. L., Laird, E. S., et al. 2009, MNRAS, 397, 623
Georgakakis, A., Nandra, K., Laird, E. S., et al. 2007, ApJ, 660, 15
Gilli, R., Daddi, E., Zamorani, G., et al. 2005, A&A, 430, 811
Gilli, R., et al. 2009, A&A, 494, 33
Hasinger, G., Cappelluti, N., Brunnen, H. et al. 2007, ApJS, 172, 29
Hasinger, G., et al. 2008, A&A, 490, 905
Hickox, R. C., Jones, C., Forman, W. R., 2009, ApJ, 696, 891
Hopkins, P.F., Hernquist, L., Cox, T.J., Keres, D., 2008, ApJ, 175, 365
Kalberla, P. M. W., et al. 2005, A&A, 440, 775
Koutoulidis, L., Plionis, M., Georgantopoulos, I., Fanidakis, N., 2013, MNRAS, 428, 1382
Krumpe, M., Miyaji, T., Coil, A. L. 2010, ApJ, 713, 558
Krumpe, M., Miyaji, T., Coil, A. L. & Aceves H. 2012, ApJ, 746, 1
Landy, S. D., & Szalay A. S., 1993, ApJ, 412, 64
Li, C., Kauffmann, G., Wang, L., et al., 2006, MNRAS, 373, 457
Marconi, A., et al. 2004, MNRAS, 351, 169
Merloni, A., & Heinz, S. 2008, MNRAS, 388, 1011
Merloni, A., Bongiorno, A., Bolzonella, M., Brusa, M, et al., 2010, ApJ, 708, 137
Miyaji, T., Zamorani, G., Cappelluti, N., et al., 2007, ApJS, 172, 396
Miyaji, T., Krumpe, M., Coil, A. L., et al. 2011, ApJ, 726, 83
Moster, Benjamin P.; Naab, Thorsten; White, Simon D. M., 2013, MNRAS428, 312
Mountrichas G. et al. 2013, MNRAS, 430, 661
Mountrichas, G., Georgakakis, A., 2012, MNRAS, 420, 514
Myers, A. D., Brunner, R. J., Richards, G. T., et al. 2007, ApJ, 658, 99
Peebles P. J. E., 1980, The Large Scale Structure of the Universe (Princeton: Princeton Univ. Press)
Salvato, M., Hasinger, G., Ilbert, O., et al., 2009, ApJ, 690, 1250
Scoville, N., Abraham, R. G., Aussel, H., et al., 2007, ApJS, 172, 38
Shankar, F., Weinberg D. H., et al. 2009, ApJ, 690, 20
Shankar F., et al., 2010, ApJ, 718, 231
Shankar F., Weinberg D. H. & Miralda-Escude J. 2013, MNRAS, 428, 421
Shankar, F.; Lapi, A.; Salucci, P.; De Zotti, G.; Danese, L., 2006, ApJ, 643, 14
Shen Y., Strauss, M. A., Ross, N. P., Hall, P. B., et al. 2009, ApJ697, 1656
Shen Y., 2009, ApJ, 704, 89
Sheth, R. K. & Tormen, G. 1999, MNRAS, 308, 119
Sheth R. K., Mo H. J., Tormen G. 2001, MNRAS, 323, 1
Starikova, S. et al., 2011, ApJ, 741, 15
Tinker, J. L., Weinberg, D. H., Zheng, Z., Zehavi, I., ApJ, 631, 41
Tozzi, P., et al. 2006, A&A, 451, 457
van den Bosch, F. C., 2002, MNRAS, 331, 98
Vittorini, V.; Shankar, F.; Cavaliere, A., 2005, MNRAS, 363, 1376